Efficient and Robust Dynamic Simulation of Power Systems with Holomorphic Embedding

Rui Yao, *Member, IEEE,* Yang Liu, *Student Member, IEEE,* Kai Sun, *Senior Member, IEEE,* Feng Qiu, *Senior Member, IEEE,* and Jianhui Wang, *Senior Member, IEEE*

***Abstract*—Dynamic simulation is vitally important in power system analysis, but traditional approaches based on numerical integration over small time steps are time-consuming. Also, the Newton-Raphson method suffers from difficulty in convergence when solving nonlinear algebraic equations. This paper proposes a novel dynamic simulation approach based on holomorphic embedding. By obtaining a high-order approximation of system dynamics, it achieves a much larger time step and thus enhances the computational efficiency significantly. In addition, the new approach avoids non-convergence issues in solving algebraic equations, which improves robustness. The approach includes flexible modeling of synchronous generators and controllers, and we propose a method for modeling generator coordinate transformations. The approach is tested on the IEEE 39-bus, 10-generator system and a Polish 2383-bus, 327-generator system. The results demonstrate promising computational efficiency and satisfactory numerical robustness for the analysis of large-scale power systems.**

***Index Terms*—Dynamic simulation, stability, convergence, load model, synchronous generator, contingency, analytical solution**

I. Introduction

MODERN power systems are large in scale and complex in composition (including transmission lines, transformers, generators, loads, and controllers). The complex structure and diverse element behavior may bring various security issues. Of the approaches for stability analysis, in contrast to the specified analysis methods that are usually subject to simplifications and assumptions [1]–[3], dynamic simulation is a generic approach for dynamic security analysis (DSA) [4]–[7] of power systems due to its flexibility in accommodating various elements, control measures, and disturbances.

Mathematically, dynamic simulation solves the initial-value problem (IVP) of differential-algebraic equations (DAE). Conventional approaches commonly used by commercial software that include explicit and implicit methods [4], [8] approximate the trace of state variables as numerical integration of differential equations with small time steps. Because numerical integration is a low-order approximation of system dynamics, the time step should be small enough to confine the error, which limits the speed of the simulation. To enhance performance, it is desirable to develop novel methodologies that extend time steps and decrease errors.

Moreover, complex nonlinear dynamic behaviors also pose challenges for simulation. To simplify computation, many dynamic simulation algorithms assume that loads use a constant-impedance model [9]–[11], which makes the DAE convertible to ordinary differential equations (ODE). However, the actual load behaviors may be quite different from those of constant impedance loads, and such an assumption may cause substantial errors in DSA [12], [13]. More accurate modeling of load behaviors leads to nonlinearity in algebraic equations, and conventional approaches usually use the Newton-Raphson method to solve the equations. However, the Newton-Raphson method depends on the selection of the initial guess: it may fail to converge when the system is large, or the system is in stress, or the disturbance is relatively large.

In recent years, the holomorphic embedding (HE) [14] has become a promising methodology for power system analysis. It was initially proposed as an efficient and robust approach for steady state analysis, which has been used for solving stressed power flow [15], voltage security analysis (VSA) [16], network reduction [17], and power flow with FACTS devices [18]. HE is also utilized in probabilistic power flow [19] and remote voltage control [20]. HE is further extended to study dynamic voltage security [21], which achieves much larger time steps and avoids non-convergence issues. However, ref. [21] does not consider synchronous generators, and the method cannot be directly applied to model synchronous generators because the transformation between generator and network coordinates has sinusoidal functions, which cannot apply the method from ref. [21]. Moreover, ref. [21] only considers continuous increase of load and generation in VSA, but does not consider faults. Many instability events are caused by faults, so it is important to analyze the dynamic security under faults efficiently and robustly.

This paper proposes an efficient and robust approach for dynamic simulation in power systems based on holomorphic embedding. The paper first proposes generic rules for deriving HE formulation and solving HE approximate solutions of DAE. Then, by introducing the generator interface, HE formulations of synchronous generators and the coordinate transformation, and the HE formulation of power system dynamics are established. The instant switches in power systems caused by faults are also modeled and solved by HE. By putting together the HE formulations for solving system dynamics and instant

This work was supported in part by the ERC Program of the NSF and DOE under NSF grant EEC-1041877, in part by NSF grant ECCS-1610025 and in part by DOE Advanced Grid Modeling Program grant DE-OE0000875. (*Corresponding author: Kai Sun*)

R. Yao is with Argonne National Laboratory, Lemont, IL 60439 and University of Tennessee, Knoxville, TN 37996 (email: ryao@anl.gov).

K. Sun and Y. Liu are with University of Tennessee, Knoxville, TN 37996 (emails: kaisun@utk.edu, yliu161@vols.utk.edu).

F. Qiu is with Argonne National Laboratory, Lemont, IL 60439 (email: fqiu@anl.gov).

J. Wang is with Southern Methodist University, Dallas, TX 75275 (email: jianhui@smu.edu).

switches, the overall dynamic simulation process based on HE is established. The contributions of this paper are four-fold: 1) General rules for deriving and solving HE formulation of DAE in power systems are proposed; 2) The models of synchronous generators and controllers in HE formulation are established through a flexible generator interface; 3) The transformation between generator and network coordinates is modeled and solved with HE; 4) The HE formulation of instant switches in power systems is proposed and solved.

The rest of the paper is organized as follows. Section II proposes generic rules for deriving and solving HE formulations for DAE. Section III establishes HE formulation of power system dynamics, and elucidates the modeling of synchronous generators and coordinate transformation. Section IV proposes the HE formulation for solving system states at post-fault instant. Section V puts together the HE for solving system dynamics and instant-switches, and establishes a full solution for dynamic simulation based on HE. Section VI consists of test cases on 2-bus system, an IEEE 39-bus system and a Polish 2383-bus system. Section VII is the conclusion.

II. Holomorphic embedding in time domain

A. Dynamic simulation of power systems

The dynamic simulation of a power system typically solves a set of DAE:

$$\dot{\mathbf{x}} = \mathbf{f}(\mathbf{x}, \mathbf{y}, \mathbf{p}(t)), \tag{1a}$$

$$\mathbf{0} = \mathbf{g}(\mathbf{x}, \mathbf{y}, \mathbf{p}(t)), \tag{1b}$$

where $\mathbf{x}$ denotes state variables, $\mathbf{y}$ stands for algebraic variables (e.g., voltage phasors on the buses), and $\mathbf{p}(t)$ denotes system configuration (e.g., the connection status of branches, the extent of load increase). The disturbances introduced into a power system can be represented by changing $\mathbf{p}(t)$. In this paper, the bold variables denote vectors or matrices.

In a numerical integration method for solving DAE, with a known system state at time t (i.e., $\mathbf{x}(t)$ and $\mathbf{y}(t)$), and given a time step Δt, the next-step state $\mathbf{x}(t+\Delta t)$ is approximated as the following discrete form:

$$\mathbf{x}(t+\Delta t) = \mathbf{x}(t) + \Delta \mathbf{x}_t, \tag{2}$$

where $\Delta \mathbf{x}_t$ is an approximated increment of $\mathbf{x}$ based on (1a). Such a scheme introduces error at level $O(\Delta t^{k+1})$, and k is usually up to 5 (e.g., modified Euler method with $k=2$ and Runge-Kutta method with $k=4$). Methods with $k>5$ also exist but are less frequently used because they are difficult to derive, and many more computation sub-steps are needed to increase the order k which affects the efficiency. Therefore, the commonly-used numerical integration methods are low-order approximations, which confine the time step Δt. Moreover, solving (1) also includes solving algebraic equations (AE) (1b), but the Newton method may fail to converge. To improve the efficiency and the robustness of dynamic simulation, a higher-order approximation of DAE with improved convergence is desirable. In the following sections, the holomorphic embedding (HE) will be utilized to solve the DAE of power systems with arbitrarily higher-order approximations.

B. Approximation with holomorphic embedding

For an IVP in the complex domain:

$$0 = h\left(\frac{\mathrm{d}z(\alpha)}{\mathrm{d}\alpha}, z(\alpha), \alpha\right),\ \alpha \in \mathbb{C}, z(0) = z_0, \tag{3}$$

where h is a holomorphic (infinitely differentiable in complex domain) function. HE solves z as a power series $\sum_{k=0}^{\infty} z[k]\alpha^k$, and the series converges to $z(\alpha)$ within a radius R_z:

$$z(\alpha) = \sum_{k=0}^{\infty} z[k]\alpha^k, |\alpha| < R_z. \tag{4}$$

Therefore, within the convergence radius R_z, the truncated power series $\sum_{k=0}^{N_L} z[k]\alpha^k$ is a reasonable approximation of $z(\alpha)$. In the following contents of this paper, we use variables with square-bracketed integers (e.g. $z[k]$) to denote the coefficients of power series. Moreover, the Padé approximant is a common post-processor of power series to further expand the usable region of approximation [22]. For the truncated power series $\sum_{k=0}^{N_L} z[k]\alpha^k$, the Padé approximant has the following form:

$$[m/n]_z(\alpha) = \frac{a_{z0} + a_{z1}\alpha + \cdots + a_{zm}\alpha^m}{1 + b_{z1}\alpha + \cdots + b_{zn}\alpha^n}, \tag{5}$$

where $m+n=N_L$. It is recommended that m and n are as close as possible to achieve a best convergence region [23].

As for solving problems in power systems, the embedded variable α is usually a real variable. Because $\mathbb{R} \subset \mathbb{C}$, the power series (4) and Padé approximant (5) still hold for $\alpha \in \mathbb{R}$. Holomorphic embedding has been used to solve power flows [24] and static voltage security analysis [16]. In those steady-state studies, the embedded variable α either connects the desired solution from a trivial solution without physical meaning, or is an implicit representation of time. In dynamic studies, the time t can be explicitly used as the embedded variable. In power systems, the DAE (1) is holomorphic in segments, which means that in each segment without the occurrence of a singularity, the solutions $x(t)$ and $y(t)$ can be asymptotically approximated by their Taylor series. Thus, for the DAE of power systems (1) with initial values $x(0)$ and $y(0)$, in the time interval with continuous $p(t)$, we can use HE to obtain approximate solutions as truncated series:

$$x(t) \approx \sum_{k=0}^{N_L} x[k]t^k,\ y(t) \approx \sum_{k=0}^{N_L} y[k]t^k, \tag{6}$$

or the corresponding Padé approximants.

C. Basic rules for deriving HE

As (4) shows, the computation of HE is to derive the coefficients $z[k]$ that correspond to the studied variable $z(\alpha)$. The equations of the HE coefficients can be derived from the original DAE by following some rules. Assume that the studied DAE only contains the following operations:

1) Linear operations e.g. $az(\alpha)+b$, where a, b are constants;
2) Multiplication of variables, such as $z_1(\alpha)z_2(\alpha)$; and
3) Derivatives, such as $\frac{\mathrm{d}z(\alpha)}{\mathrm{d}\alpha}$.

Many equations can be converted to formulas that only contain the above operations. For example, the division operation can be eliminated by multiplying the denominator on both sides of the equation. More complex operations, such as sinusoidal functions, can be approximately converted to polynomials (also multiplication) with truncated Taylor series (see Section III). After converting the equations from the original DAE into the formulas using the above operations, the terms in the equations of HE coefficients can be derived following the rules listed in Table I.

TABLE I
MATHEMATICAL OPERATIONS AND CORRESPONDING HE

Operations	Original form	kth-order HE coefficient
Linear	$az(\alpha)+b$	$az[k]+b$
Multiplication	$z_1(\alpha)\cdots z_m(\alpha)$	$\sum_{\sum k_i=k} z_1[k_1]\cdots z_m[k_m]$
Derivative	$\frac{\mathrm{d}z(\alpha)}{\mathrm{d}\alpha}$	$(k+1)z[k+1]$

By using the rules in Table I, the HE can be solved by gathering all the terms in the equations. To better illustrate the derivation of HE, a simple example DAE is shown:

$$\frac{\mathrm{d}z_1(\alpha)}{\mathrm{d}\alpha} = 2z_1(\alpha)z_2(\alpha) + z_1(\alpha) \tag{7a}$$

$$0 = z_2(\alpha)^2 + z_1(\alpha) - 1\ . \tag{7b}$$

From Table I, the equations of HE coefficients are derived:

$$(k+1)z_1[k+1] = 2\sum_{i=0}^{k} z_1[i]z_2[k-i] + z_1[k] \tag{8a}$$

$$0 = \sum_{i=0}^{k} z_2[i]z_2[k-i] + z_1[k] - f_\delta(k,0)\ , \tag{8b}$$

where $f_\delta(i,j)=1$ only if $i=j$, and otherwise $f_\delta(i,j)=0$.

Algorithm 1. General procedures for solving DAEs with HE.

Input: DAE (e.g. eq. (7)), initial states $\mathbf{x}_0$, $\mathbf{y}_0$, maximum HE order N_L.
Output: HE coefficients $\mathbf{x}[k]$, $\mathbf{y}[k]$, $k=0,\cdots,N_L$.

1 $k \leftarrow 0$, $\mathbf{x}[0] \leftarrow \mathbf{x}_0$, $\mathbf{y}[0] \leftarrow \mathbf{y}_0$.
2 **while** $k < N_L$ **do**
3 $k \leftarrow k+1$.
4 Obtain equations for HE coefficients at kth order based on the rules in Table I (e.g. (8)).
5 Calculate $\mathbf{x}[k]$ from HE coefficient equations of differential equations (e.g. (8a)) by using $\mathbf{x}[i]$, $\mathbf{y}[i]$, $i=0,\cdots,k-1$.
6 Solve $\mathbf{y}[k]$ from HE coefficient equations of algebraic equations (e.g. (8b)) by using $\mathbf{x}[i]$, $i=0,\cdots,k$, and $\mathbf{y}[i]$, $i=0,\cdots,k-1$.
7 **end while**.

In differential equations, the higher-order coefficients (e.g. $z_1[k+1]$ in (8a)) can be directly calculated by using the lower-order coefficients (coefficients of z_1 and z_2 of up to the kth order). While in algebraic equations, because level-0 coefficients are already known in IVP, the highest-order coefficients (e.g. $z_1[k]$ and $z_2[k]$ in (8b)) have linear relationships. Therefore, solving the nonlinear DAEs is transformed to solving the linear equations of HE coefficients, which avoids the numerical problems in solving nonlinear equations directly. When solving large-scale DAEs, solving the linear equations will be the major bottleneck of performance, but note that the coefficient matrix of the linear equations is constant, which only needs factorization once. The Algorithm 1 describes an iterative procedure for solving DAEs with HE.

D. Multi-stage HE

The approximants of time-domain solution of DAE derived by HE have limited convergence radius, in other words, the solution approximately satisfies the DAE only within an interval in the time domain. Also, the step length is limited if the system hits non-smoothness (e.g. limiters, model switches). To reach the desired simulation length, a multi-stage scheme is used. The entire time-domain solution is connected by multiple segments of solutions derived by HE. In each stage, the imbalance of DAE is checked along the HE solutions. Generally, for a DAE with the form of (3):

$$\mathbf{0} = \mathbf{h}\left(\frac{\mathrm{d}\mathbf{z}(t)}{\mathrm{d}t}, \mathbf{z}(t), t\right). \tag{9}$$

Assume the approximate solution based on HE to be

$$\tilde{\mathbf{z}}(t) = \sum_{k=0}^{N_L} \tilde{\mathbf{z}}[k]t^k, \tag{10}$$

and then we can derive:

$$\frac{\mathrm{d}\tilde{\mathbf{z}}(t)}{\mathrm{d}t} = \sum_{k=1}^{N_L} k\tilde{\mathbf{z}}[k]t^{k-1}. \tag{11}$$

Both (10) and (11) are truncated power series and can be further converted to Padé approximations. Here we take the power-series approximate solutions (10) and (11) as an example. The imbalance of the DAE is derived by substituting (10) and (11) into the right-hand side of (9), and calculating the difference between the two sides:

$$\mathbf{\Delta}(t) = \mathbf{0} - \mathbf{h}\left(\frac{\mathrm{d}\tilde{\mathbf{z}}(t)}{\mathrm{d}t}, \tilde{\mathbf{z}}(t), t\right). \tag{12}$$

Define $\Delta(t) = \|\mathbf{\Delta}(t)\|_\infty$. The furthest time point $t_{\max}$ satisfying $\Delta(t) < \varepsilon_E, t \le t_{\max}$ can be efficiently identified with binary search and is set as the initial-value point of the next stage. The interval between the initial-value point and $t_{\max}$ is regarded as the effective HE step. The multi-stage HE can also accurately identify the non-smooth switching events. By iteratively solving the initial-value problems, the entire time-domain solution can be obtained.

III. HE FORMULATION OF TIME-DOMAIN SIMULATION

A. Network equations

Ref. [21] proposes an HE formulation without synchronous generators. For power systems with synchronous generators, the HE formulation can be written as:

$$(P_i(t) - jQ_i(t))W_i^*(t) - \sum_l Y_{il}V_l(t) - I_{Li}(t) + I_{Gi}(t) = 0, \tag{13}$$

where V_i is the voltage phasor on bus i, whose reciprocal is W_i. Y_{il} is the element of row i and column l in the admittance matrix $\mathbf{Y}$. The constant-PQ loads are included in P_i and Q_i terms (positive values denote generations and negative values denote loads), while the constant-impedance loads are merged into $\mathbf{Y}$. The current of other loads (e.g., constant-current loads, induction motor loads) on bus i is represented by I_{Li}, and the current of all the synchronous machines is represented by I_{Gi}. Such a flexible current interface enables modular design of the overall simulation framework in which different components can be modeled in HE separately and then assembled for simulation. Also, such a design is convenient for accommodating user-defined models. All the phasors (i.e., voltage and current) are modeled in the network x-y coordinates. The generator buses use synchronous generator models instead of PV buses. From (13), the HE coefficients satisfy the equations:

$$\begin{bmatrix} -\mathbf{G} & \mathbf{B} & \mathcal{D}(\mathbf{P}[0]) & -\mathcal{D}(\mathbf{Q}[0]) \\ -\mathbf{B} & -\mathbf{G} & -\mathcal{D}(\mathbf{Q}[0]) & -\mathcal{D}(\mathbf{P}[0]) \\ \mathcal{D}(\mathbf{W}_x[0]) & -\mathcal{D}(\mathbf{W}_y[0]) & \mathcal{D}(\mathbf{V}_x[0]) & -\mathcal{D}(\mathbf{V}_y[0]) \\ \mathcal{D}(\mathbf{W}_y[0]) & \mathcal{D}(\mathbf{W}_x[0]) & \mathcal{D}(\mathbf{V}_y[0]) & \mathcal{D}(\mathbf{V}_x[0]) \end{bmatrix} \begin{bmatrix} \mathbf{V}_x[n] \\ \mathbf{V}_y[n] \\ \mathbf{W}_x[n] \\ \mathbf{W}_y[n] \end{bmatrix}$$
$$= \begin{bmatrix} \Re\left(-\sum_{k=1}^{n} \mathbf{P}[k] \circ \mathbf{W}^*[n-k] + j\sum_{k=1}^{n} \mathbf{Q}[k] \circ \mathbf{W}^*[n-k] + \mathbf{I}_L[n] - \mathbf{I}_G[n]\right) \\ \Im\left(-\sum_{k=1}^{n} \mathbf{P}[k] \circ \mathbf{W}^*[n-k] + j\sum_{k=1}^{n} \mathbf{Q}[k] \circ \mathbf{W}^*[n-k] + \mathbf{I}_L[n] - \mathbf{I}_G[n]\right) \\ \Re\left(-\sum_{k=1}^{n-1} \mathbf{W}[k] \circ \mathbf{V}[n-k]\right) \\ \Im\left(-\sum_{k=1}^{n-1} \mathbf{W}[k] \circ \mathbf{V}[n-k]\right) \end{bmatrix}, \quad (14)$$

where $\mathbf{G}$ and $\mathbf{B}$ are real and imaginary parts of $\mathbf{Y}$. $\mathbf{V}_x[n]$ and $\mathbf{V}_y[n]$ are real and imaginary parts of $\mathbf{V}[n]$. $\mathbf{W}_x[n]$ and $\mathbf{W}_y[n]$ are real and imaginary parts of $\mathbf{W}[n]$. $\Re(\cdot)$ and $\Im(\cdot)$ are real and imaginary operators, $\mathcal{D}(\cdot)$ means diagonal matrix, "$\circ$" means element-wise product. Here, other than the load current interface $\mathbf{I}_L$, the generator current is also modeled as an interface denoted as $\mathbf{I}_G$. If $\mathbf{I}_L[n]$ and $\mathbf{I}_G[n]$ are given, then $\mathbf{V}_x[n]$, $\mathbf{V}_y[n]$, $\mathbf{W}_x[n]$ and $\mathbf{W}_y[n]$ can be solved.

B. Synchronous generator

To realize a more generic dynamic simulation, we propose the HE modeling of synchronous generator and its controllers. There are several kinds of dynamic models of synchronous generators in different orders. For example, the more detailed commonly used 6th-order model [25] is shown as

$$\dot{\delta}_i = \omega_s \omega_i \quad (15a)$$
$$\dot{\omega}_i = \frac{1}{2H_i}(T_{Mi} - T_{Ei} - D_i\omega_i) \quad (15b)$$
$$T_{Ei} = V_{di}I_{di} + V_{qi}I_{qi} + (I_{di}^2 + I_{qi}^2)R_{si} \quad (15c)$$
$$\dot{e}'_{qi} = \left(-e'_{qi} - (X_{di} - X'_{di} - \gamma_{di})\, I_{di} + \left(1 - \frac{T_{AAi}}{T'_{di0}}\right) V_{fi}\right) / T'_{di0} \quad (15d)$$
$$\dot{e}'_{di} = \left(-e'_{di} + \left(X_{qi} - X'_{qi} - \gamma_{qi}\right) I_{qi}\right) / T'_{qi0} \quad (15e)$$
$$\dot{e}''_{qi} = \left(-e''_{qi} + e'_{qi} - (X'_{di} - X''_{di} + \gamma_{di})\, I_{di} + \frac{T_{AAi}}{T'_{di0}} V_{fi}\right) / T''_{di0} \quad (15f)$$
$$\dot{e}''_{di} = \left(-e''_{di} + e'_{di} + \left(X'_{qi} - X''_{qi} + \gamma_{qi}\right) I_{qi}\right) / T''_{qi0} \quad (15g)$$
$$0 = R_{si}I_{qi} + V_{qi} + X''_{di}I_{di} - e''_{qi} \quad (15h)$$
$$0 = R_{si}I_{di} + V_{di} - X''_{qi}I_{qi} - e''_{di} \quad (15i)$$
$$\gamma_{di} = \frac{T''_{di0}}{T'_{di0}} \frac{X''_{di}}{X'_{di}} (X_{di} - X'_{di}), \gamma_{qi} = \frac{T''_{qi0}}{T'_{qi0}} \frac{X''_{qi}}{X'_{qi}} (X_{qi} - X'_{qi}), \quad (15j)$$

where for a generator numbered as i, δ_i is the rotor angle, and ω_i is the per-unit rotor slip under base nominal value ω_s. H_i is the time constant of the rotor, T_{Mi} is the mechanical torque input to the generator, T_{Ei} is the electric torque, and D_i is the damping coefficient of the rotor. Four quantities describe the electromagnetic fields on the generator's own d-q coordinates, which are the transient potentials e'_{di} and e'_{qi}, and the sub-transient potentials e''_{di} and e''_{qi}. The corresponding four differential equations are (15d)-(15g). Accordingly, the current and voltage phasors on the stator are described by their components on the d- and q-axes as I_{di}, I_{qi}, V_{di}, and V_{qi}. The excitation field potential is V_{fi}. The armature resistance is R_{si}, the synchronous, transient, subtransient reactances on d- and q-axes are X_{di}, X'_{di}, X''_{di}, X_{qi}, X'_{qi}, and X''_{qi}. Moreover, the transient and subtransient time constants of equivalent coils on the d- and q-axes are T'_{di0}, T''_{di0} T'_{qi0} and T''_{qi0}. There is also a time constant of additional leakage on d-axis, T_{AAi}.

In eq. (15), the state variables are δ_i, ω_i, e'_{di}, e'_{qi}, e''_{di}, and e''_{qi}. T_{Mi} and V_{fi} are input variables, which can be obtained from the turbine governor and the exciter, respectively. The T_{Ei}, I_{di}, and I_{qi} can be eliminated with (15c), (15h), and (15i). V_{di} and V_{qi} connect to the external network.

C. Treating transformation of coordinates

In (15), each generator uses its own d-q coordinates, which is fixed on the rotor. While for the power grid, a reference phasor should be designated, whose real and imaginary parts act as the x-y coordinates of the network (see Fig. 1). Thus, when modeling the synchronous generators and the network, a transformation between the generator d-q coordinates and the network x-y coordinates is needed.

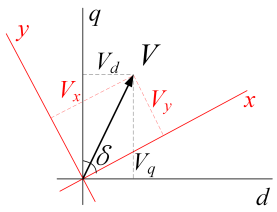

Fig. 1. d-q and x-y coordinates.

Denote the rotor angle as δ_i, the voltage (and the same for current) under two coordinates has the following transformation. Evidently, the transformation matrix $\mathbf{M}(\delta_i)$ depends on the rotor angle δ_i, and it has sinusoidal functions of δ_i:

$$\begin{bmatrix} V_{xi} \\ V_{yi} \end{bmatrix} = \begin{bmatrix} \sin\delta_i & \cos\delta_i \\ -\cos\delta_i & \sin\delta_i \end{bmatrix} \begin{bmatrix} V_{di} \\ V_{qi} \end{bmatrix} \stackrel{\text{def}}{=} \mathbf{M}(\delta_i) \begin{bmatrix} V_{di} \\ V_{qi} \end{bmatrix} \quad (16a)$$
$$\begin{bmatrix} V_{di} \\ V_{qi} \end{bmatrix} = \begin{bmatrix} \sin\delta_i & -\cos\delta_i \\ \cos\delta_i & \sin\delta_i \end{bmatrix} \begin{bmatrix} V_{xi} \\ V_{yi} \end{bmatrix} = \mathbf{M}(\delta_i)^{\mathrm{T}} \begin{bmatrix} V_{xi} \\ V_{yi} \end{bmatrix}. \quad (16b)$$

The HE formulations of sinusoidal functions are not straightforward, here an approximation is adopted for deriving the HE of $\sin\delta_i$ and $\cos\delta_i$. Select a δ_{i0} in the vicinity of the variation interval of δ_i, and choose an approximation order

m (3 or 4 is recommended), then $\sin\delta_i$ and $\cos\delta_i$ can be approximated with truncated Taylor series:

$$\cos\delta_i \approx \kappa_i \overset{\text{def}}{=} \sum_{k=0}^{m} a_k(\delta_{i0})\delta_i^k,\ \ \sin\delta_i \approx \sigma_i \overset{\text{def}}{=} \sum_{k=0}^{m} b_k(\delta_{i0})\delta_i^k. \quad (17)$$

Thus, the sinusoidal functions can be approximated by polynomials, and the rules for deriving HE formulations listed in Table I can be utilized. Note that both interface current and voltage need to do coordinate transformations. Theoretically there are two ways of introducing the transform, as (16) shows. However, since κ_i and σ_i are polynomial approximations to the sinusoidal function, the transformations are not exactly interchangeable. Therefore, we should be careful when selecting the transformations of current and voltage. When transforming between d-q coordinates and x-y coordinates, the power should be the same, in other words:

$$V_{di}I_{di} + V_{qi}I_{qi} = V_{xi}I_{xi} + V_{yi}I_{yi}. \quad (18)$$

If the current uses transformation (16b)

$$\begin{bmatrix} I_{di} \\ I_{qi} \end{bmatrix} = \begin{bmatrix} \sigma_i & -\kappa_i \\ \kappa_i & \sigma_i \end{bmatrix} \begin{bmatrix} I_{xi} \\ I_{yi} \end{bmatrix}, \quad (19)$$

according to (18), the voltage should use transformation (16a):

$$\begin{bmatrix} V_{xi} \\ V_{yi} \end{bmatrix} = \begin{bmatrix} \sigma_i & \kappa_i \\ -\kappa_i & \sigma_i \end{bmatrix} \begin{bmatrix} V_{di} \\ V_{qi} \end{bmatrix}. \quad (20)$$

Because otherwise, the invariance of power (18) is not satisfied because $\sigma_i^2+\kappa_i^2 \neq 1$. Therefore, transformations (19) and (20) are used in this paper. HE suggests that δ_{i0} be selected as the initial value of δ_i, and thus $\delta_{i0} = \delta[0]$. Also $\kappa_i[0] = \cos\delta_{i0}$, $\sigma_i[0] = \sin\delta_{i0}$. Then the HE coefficients of (19) and (20) are

$$\begin{bmatrix} I_{xi}[n] \\ I_{yi}[n] \end{bmatrix} = \begin{bmatrix} \sigma_i[0] & \kappa_i[0] \\ -\kappa_i[0] & \sigma_i[0] \end{bmatrix} \begin{bmatrix} I_{di}[n] - \sum_{k=1}^{n}\sigma_i[k]I_{xi}[n-k] + \sum_{k=1}^{n}\kappa_i[k]I_{yi}[n-k] \\ I_{qi}[n] - \sum_{k=1}^{n}\kappa_i[k]I_{xi}[n-k] - \sum_{k=1}^{n}\sigma_i[k]I_{yi}[n-k] \end{bmatrix}, \quad (21)$$

$$\begin{bmatrix} V_{di}[n] \\ V_{qi}[n] \end{bmatrix} = \begin{bmatrix} \sigma_i[0] & -\kappa_i[0] \\ \kappa_i[0] & \sigma_i[0] \end{bmatrix} \begin{bmatrix} V_{xi}[n] - \sum_{k=1}^{n}\sigma_i[k]V_{di}[n-k] - \sum_{k=1}^{n}\kappa_i[k]V_{qi}[n-k] \\ V_{yi}[n] + \sum_{k=1}^{n}\kappa_i[k]V_{di}[n-k] - \sum_{k=1}^{n}\sigma_i[k]V_{qi}[n-k] \end{bmatrix}. \quad (22)$$

When solving the system dynamics with synchronous generators, take 6th-order generator model as an example. From (15h) and (15i) we can obtain

$$\begin{aligned} 0 &= R_{si}I_{qi}[n] + V_{qi}[n] - e''_{qi}[n] + X''_{di}I_{di}[n] \\ 0 &= R_{si}I_{di}[n] + V_{di}[n] - e''_{di}[n] - X''_{qi}I_{qi}[n] \end{aligned}, \quad (23)$$

where $e''_{di}[n]$ and $e''_{qi}[n]$ are first derived from (15g) and (15f), respectively. Then $I_{di}[n]$, $I_{qi}[n]$, $V_{di}[n]$, $V_{qi}[n]$, $I_{xi}[n]$ and $I_{yi}[n]$ can be eliminated from (14), (21), (22) and (23), and then the coefficients of bus voltage $\mathbf{V}_x[n]$, $\mathbf{V}_y[n]$ are solved.

D. Controllers on synchronous generators

The synchronous generators are equipped with various controllers, such as automatic voltage regulators (AVR) and turbine governors (TG). When modeling the synchronous generators, it is necessary to model these controllers also. As examples, one AVR model and one TG model are listed in this paper. The TG uses the Type-II TG model in ref. [25]:

$$\dot{t}_{gi} = (\frac{1}{R_i}(1 - \frac{T_{gi1}}{T_{gi2}})(\omega_{i\text{ref}} - \omega_i) - t_{gi})/T_{gi2} \quad (24a)$$

$$T^*_{Mi} = t_{gi} + \frac{1}{R_i}\frac{T_{gi1}}{T_{gi2}}(\omega_{i\text{ref}} - \omega_i) + T_{Mi0} \quad (24b)$$

$$T_{Mi} = L(T^*_{Mi}, T_{i\max}, T_{i\min}) \overset{\text{def}}{=} \begin{cases} T_{i\min}, T^*_{Mi} < T_{i\min} \\ T^*_{Mi}, T^*_{Mi} \in [T_{i\min}, T_{i\max}] \\ T_{i\max}, T^*_{Mi} > T_{i\max} \end{cases}, \quad (24c)$$

and the AVR uses the Type-III model in ref. [25]:

$$\dot{v}_{mi} = (V_i - v_{mi})/T_{ri} \quad (25a)$$

$$\dot{v}_{ri} = (\mu_{0i}(1 - \frac{T_{vi1}}{T_{vi2}})(V_{i\text{ref}} - v_{mi}) - v_{ri})/T_{vi2} \quad (25b)$$

$$\dot{v}_{fi} = ((v_{ri} + \mu_{0i}\frac{T_{vi1}}{T_{vi2}}(V_{i\text{ref}} - v_{mi}) + v_{fi0})\frac{V_i}{V_{0i}} - v_{fi})/T_{ei} \quad (25c)$$

$$V_{fi} = L^{NW}(v_{fi}, V_{fi\max}, V_{fi\min}). \quad (25d)$$

Then the corresponding HE formulations can be derived based on the rules introduced in Section II.C. Note that there is a non-differentiable limiter function $L(\cdot)$ and non-windup limiter function $L^{NW}(\cdot)$ in the AVR and TG models, which cannot be entirely converted into HE formulation. To address such a problem, the HE is formulated only in the vicinity of the initial value (i.e., only the segment where the initial value is located is considered). Since multi-stage HE is adopted, when the variable goes beyond the segment, the switching event will be detected by the imbalance of the equation, and then the segment for HE approximation changes accordingly.

IV. Solve post-switch state with HE

Instant disturbances may occur in power systems, such as faults, or opening or closing of switches. As (1) shows, at the instant, the state variable $\mathbf{x}$ does not change, and as system parameters change from $\mathbf{p}(t_f^-)$ to $\mathbf{p}(t_f^+)$, the algebraic variable $\mathbf{y}$ changes accordingly. Usually the algebraic variable before disturbance $\mathbf{y}(t_f^-)$ is known, and the post-disturbance variable $\mathbf{y}(t_f^+)$ needs to be solved. The most commonly used instant disturbance in dynamic simulation is a symmetric three-phase fault. In this case, the network admittance changes from $\mathbf{Y}^-$ to $\mathbf{Y}^+$. In HE formulation, this denotes the embedded variable as α, the network algebraic equations are

$$\begin{aligned} (P_i - jQ_i)W_i^*(\alpha) - \sum_l \left(Y_{il}^- + \alpha(Y_{il}^+ - Y_{il}^-)\right)V_l(\alpha) \\ - I_{Li}(\alpha) + I_{Gi}(\alpha) = 0, \end{aligned} \quad (26)$$

then $\alpha = 0$ corresponds to $y(t_f^-)$ and $\alpha = 1$ corresponds to $y(t_f^+)$. The post-switch state can be obtained by solving the approximate solution of (26) and assigning $\alpha = 1$. The equations of HE coefficients are shown in (27).

At the instant of disturbance, the state variables are constant, and thus the equations of dynamic elements (e.g., synchronous

$$\begin{bmatrix} -\mathbf{G}^- & \mathbf{B}^- & \mathcal{D}(\mathbf{P}[0]) & -\mathcal{D}(\mathbf{Q}[0]) \\ -\mathbf{B}^- & -\mathbf{G}^- & -\mathcal{D}(\mathbf{Q}[0]) & -\mathcal{D}(\mathbf{P}[0]) \\ \mathcal{D}(\mathbf{W}_x[0]) & -\mathcal{D}(\mathbf{W}_y[0]) & \mathcal{D}(\mathbf{V}_x[0]) & -\mathcal{D}(\mathbf{V}_y[0]) \\ \mathcal{D}(\mathbf{W}_y[0]) & \mathcal{D}(\mathbf{W}_x[0]) & \mathcal{D}(\mathbf{V}_y[0]) & \mathcal{D}(\mathbf{V}_x[0]) \end{bmatrix} \begin{bmatrix} \mathbf{V}_x[n] \\ \mathbf{V}_y[n] \\ \mathbf{W}_x[n] \\ \mathbf{W}_y[n] \end{bmatrix}$$
$$= \begin{bmatrix} \Re\left(-\sum_{k=1}^{n} \mathbf{P}[k] \circ \mathbf{W}^*[n-k] + j\sum_{k=1}^{n} \mathbf{Q}[k] \circ \mathbf{W}^*[n-k] + \mathbf{I}_L[n] - \mathbf{I}_G[n]\right) \\ \Im\left(-\sum_{k=1}^{n} \mathbf{P}[k] \circ \mathbf{W}^*[n-k] + j\sum_{k=1}^{n} \mathbf{Q}[k] \circ \mathbf{W}^*[n-k] + \mathbf{I}_L[n] - \mathbf{I}_G[n]\right) \\ \Re\left(-\sum_{k=1}^{n-1} \mathbf{W}[k] \circ \mathbf{V}[n-k]\right) \\ \Im\left(-\sum_{k=1}^{n-1} \mathbf{W}[k] \circ \mathbf{V}[n-k]\right) \end{bmatrix} + \begin{bmatrix} \mathbf{G}^+ - \mathbf{G}^- & -\mathbf{B}^+ + \mathbf{B}^- \\ \mathbf{B}^+ - \mathbf{B}^- & \mathbf{G}^+ - \mathbf{G}^- \\ \mathbf{0} & \mathbf{0} \\ \mathbf{0} & \mathbf{0} \\ \mathbf{0} & \mathbf{0} \end{bmatrix} \begin{bmatrix} \mathbf{V}_x[n-1] \\ \mathbf{V}_y[n-1] \end{bmatrix} \tag{27}$$

machines and asynchronous machines) can be significantly simplified. Take synchronous machines as an example, only the algebraic equations on stators are retained and can be generalized as the following form:

$$\begin{bmatrix} \rho_{si} & -\chi_{qi} \\ \chi_{di} & \rho_{si} \end{bmatrix} \begin{bmatrix} I_{di}(\alpha) \\ I_{qi}(\alpha) \end{bmatrix} + \begin{bmatrix} V_{di}(\alpha) \\ V_{qi}(\alpha) \end{bmatrix} = \begin{bmatrix} \varepsilon_{di} \\ \varepsilon_{qi} \end{bmatrix}. \tag{28}$$

With different orders of generator models [25], the parameters are determined in Table II.

TABLE II
PARAMETERS OF SYNCHRONOUS GENERATOR STATOR EQUATIONS

Orders	ρ_{si}	χ_{di}	χ_{qi}	ε_{di}	ε_{qi}
II	R_{si}	X'_{di}	X_{qi}	E_{di}	e'_{qi}
III	R_{si}	X'_{di}	X_{qi}	E_{di}	e'_{qi}
IV	R_{si}	X'_{di}	X'_{qi}	e'_{di}	e'_{qi}
V	R_{si}	X''_{di}	X''_{qi}	e''_{di}	e''_{qi}
VI	R_{si}	X''_{di}	X''_{qi}	e''_{di}	e''_{qi}

Because rotor angle δ_i is constant at the instant of disturbance, the transformation between d-q and x-y axes is linear. Based on (28) and (16b), the equations of HE coefficients are:

$$\begin{bmatrix} \rho_{si} & -\chi_{qi} \\ \chi_{di} & \rho_{si} \end{bmatrix} \begin{bmatrix} \sin\delta_i & -\cos\delta_i \\ \cos\delta_i & \sin\delta_i \end{bmatrix} \begin{bmatrix} I_{xi}[k] \\ I_{yi}[k] \end{bmatrix} + \begin{bmatrix} \sin\delta_i & -\cos\delta_i \\ \cos\delta_i & \sin\delta_i \end{bmatrix} \begin{bmatrix} V_{xi}[k] \\ V_{yi}[k] \end{bmatrix} = \begin{bmatrix} \varepsilon_{di} \\ \varepsilon_{qi} \end{bmatrix}. \tag{29}$$

Combining (29) and (27) eliminates the I_{xi} and I_{yi} terms.

In summary, post-switch states are computed by solving the problem (26) at $\alpha = 1$. Note that multi-stage HE technique may be needed to reach the solution at $\alpha = 1$.

V. Overall Dynamic Simulation Process

With the methods introduced in Sections III and IV, the whole process of dynamic simulation can be realized. Fig. 2 illustrates the key steps for transient stability analysis. The dynamic simulation starts with a certain state (labeled as ⓪ in the figure), and then the dynamic processes (labeled ①, ②, and ③, representing the pre-fault, fault-on, and post-fault stages, respectively) are simulated with the method demonstrated in Section III until a switch occurs in the system. The post-switch states (labeled ④) need to be solved by using the method introduced in Section IV. And the post-switch states are used as the starting points of the following simulations of dynamics. The initial state of the entire simulation is usually given by the steady-state power flow. At the initial steady state, usually the system is not in stress and the solution does not deviate much from the normal state, so the conventional methods for solving power flow (e.g., Newton-Raphson method) are usually sufficient. While when solving the post-switch state, the system state may significantly deviate from the original one, and the conventional Newton-Raphson method may fail to converge. Thus, HE should be selected as a reliable method for solving the post-switch state in dynamic simulation. Fig. 3 shows the overall procedures of simulation based on HE.

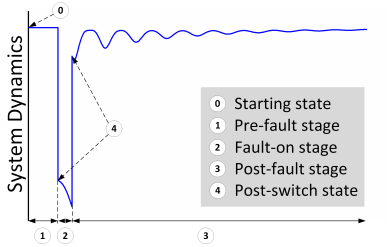

Fig. 2. Key steps in transient stability analysis

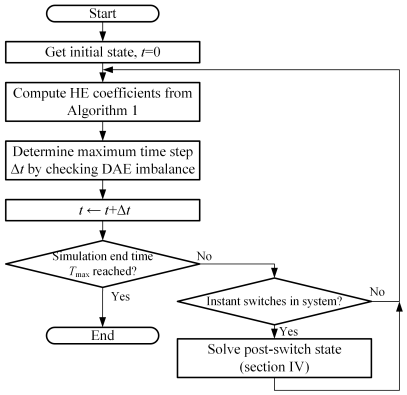

Fig. 3. Flowchart of simulation procedures based on HE.

VI. Test Cases

A. 2-bus test system

A 2-bus system (Fig. 4) is used to compare the accuracy because the real solution of such a system can be obtained

analytically. Increase the loading level λ at a constant rate $\frac{\mathrm{d}\lambda}{\mathrm{d}t} = 2t+1$ from initial value $\lambda(0) = 0$ until voltage collapse. The solution of the bus 2 voltage $V_2 = V_{2x} + jV_{2y}$ is:

$$V_{2x} = \frac{E}{2} + \sqrt{\frac{E^2}{4} - (Pr+Qx)(t^2+t) - \frac{(Qr-Px)^2}{E^2}(t^2+t)^2}$$
$$V_{2y} = \frac{Qr-Px}{E}(t^2+t), \tag{30}$$

and at $t = \sqrt{E^2\frac{\sqrt{(Pr+Qx)^2+(Qr-Px)^2}-Pr-Qx}{(Qr-Px)^2} + \frac{1}{4}} - \frac{1}{2}$, the voltage collapses. The traditional explicit methods include modified Euler (ME) and 4th-order Runge-Kutta (RK4) methods with the Newton-Raphson (NR) method for solving algebraic equations. To be concise, they are abbreviated as ME-NR and RK4-NR, respectively. Also, as a commonly used implicit method, the trapezoidal method (abbreviated as TRAP) is also tested. All the traditional methods use $\Delta t = 0.01$ s as time step. For HE, set $N_L = 30$. Set $E = 1.01$, $z = 0.01+j0.05$, and $P+jQ = 0.1+j0.3$, conduct simulation with HE and traditional methods, and compare with the real solutions in (30). Fig. 5 shows the error, and Table III shows the computation time. Results show that HE has the lowest error and fastest computation speed.

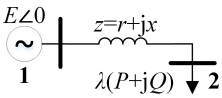

Fig. 4. 2-bus test system.

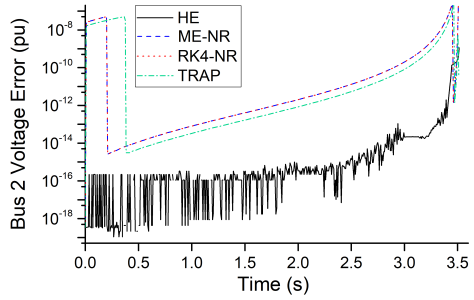

Fig. 5. Computation errors of HE and traditional methods.

TABLE III
COMPUTATION TIME OF DIFFERENT METHODS IN 2-BUS SYSTEM

Method	HE	ME-NR	RK4-NR	TRAP
time (s)	1.347	3.071	4.110	3.459

B. IEEE 39-bus system

First, the proposed approach is tested on the modified IEEE 39-bus system. The system has 10 synchronous machines, 19 PQ loads, 18 ZIP loads, and 18 induction motors. The synchronous generators use 6th-order models. A three-phase fault is applied at bus 3 at 0.5 s and is then cleared at 0.75 s. The three-phase fault is applied with a larger fault impedance of $Z_f = j0.5$. System dynamics in 10 s are simulated. The methods are developed in Matlab and are tested on laptop computer with Intel Core™ i7-6600U CPU and 8GM RAM. Fig. 6 shows the curves of voltage magnitude.

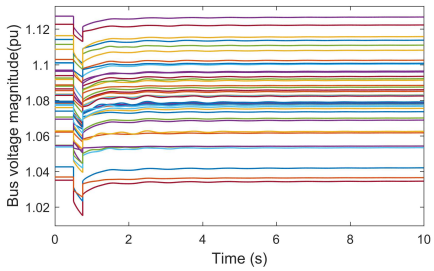

Fig. 6. Voltage magnitude curves in IEEE 39-bus system.

Table IV compares the computation time of different methods, including ME-NR, RK4-NR and TRAP with different time steps, and HE. Fig. 7 also shows the mean error of state variables in each method for comparison. To calculate the error of each method, the result from RK4-NR with a very tiny time step $\Delta t = 1 \times 10^{-5}$ s is considered as the real solution. The results show that HE has a significant advantage in both efficiency and accuracy to ME-NR, RK4-NR and TRAP. Conventional methods are expected to use very small time step ($\Delta t < 0.001$ s) to get the same error level as HE; however, in that case, the computation speed will be very slow.

TABLE IV
COMPUTATION TIME OF DIFFERENT METHODS IN IEEE 39-BUS SYSTEM

Method	Computation time (s)	Steps
ME-NR (Δt = 0.01 s)	21.58	1000
ME-NR (Δt = 0.005 s)	34.44	2000
ME-NR (Δt = 0.002 s)	84.46	5000
RK4-NR (Δt = 0.01 s)	34.64	1000
RK4-NR (Δt = 0.005 s)	64.78	2000
RK4-NR (Δt = 0.002 s)	156.37	5000
TRAP (Δt = 0.01 s)	24.34	1000
TRAP (Δt = 0.005 s)	36.02	2000
TRAP (Δt = 0.002 s)	95.51	5000
HE ($N_L = 30$)	4.49	54

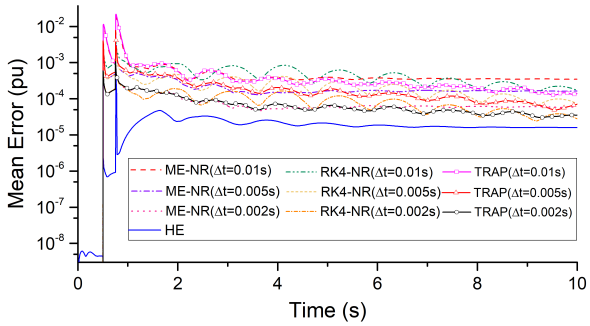

Fig. 7. Comparison of errors (symbols do not represent actual steps).

There are also variable step control schemes for the conventional methods that may speed up computation. But using

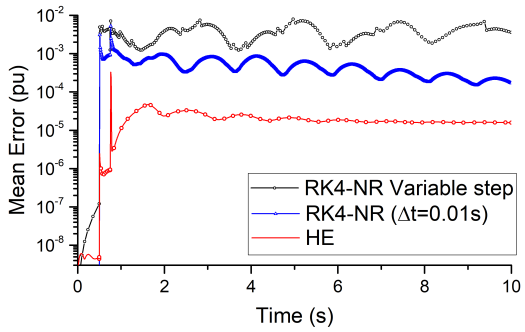

Fig. 8. Errors of variable-step RK4-NR, fixed-step RK4-NR and HE.

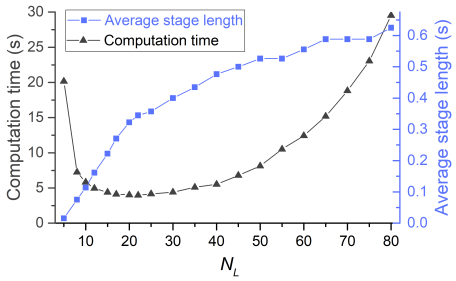

Fig. 9. Computation time and average stage length under different N_L.

larger time step may further decrease accuracy. The numerical experiment is also performed with the adaptive-step-length 4th-order Runge-Kutta method [26] in the same testing environment. The variable-step RK4 method uses minimum step length as 10^{-5} s and maximum step length as 0.5 s. The step-doubling scheme [26] is used to estimate the error, and the step length amplifies or shrinks once the estimated error is too small or too large. The initial step length is 0.01 s. Fig. 8 shows the comparison of error among variable-step RK4-NR, fixed-step RK4-NR (Δt = 0.01 s) and HE. The benchmark method is also the RK4-NR with a tiny time step $\Delta t = 10^{-5}$ s. The variable-step RK4-NR uses 201 steps to finish computation, where the smallest step is about 0.0036 s (at the beginning of the post-fault stage), and the largest step is about 0.075 s (at the end of the simulation). The results show that variable-step RK4-NR uses significantly fewer steps than fixed-step RK4-NR, but it sacrifices accuracy: its mean error is about 10 times that of the fixed-step counterpart. In addition, the error estimation and step control scheme costs extra computational resources. Although the average time-step length of variable-step RK4-NR is 5 times that of the fixed-step method, the variable-step RK4-NR takes 21.25 s, which only saves about 39% of computation time. Compared with variable-step and fixed-step RK4-NR methods, HE has advantage both in accuracy and computational efficiency.

The parameter N_L in HE influences the computational speed. The larger N_L is, the more computation is needed in each HE approximation. In the meantime, the effective range of HE approximation also enlarges with the increase of N_L, and thus fewer stages will be needed. Therefore, there might be a best N_L to achieve the least computation time. In this simulation configuration, different N_L values are tested. Fig. 9 shows the computation time as well as the average length of HE stages. The result indicates that the effective range of HE approximation grows as N_L increases; however, as the time consumption in each HE stage rises, the total computation time first drops and then increases. In this case, selecting a N_L value between 15 and 30 yields the best computation performance.

The previous test selects a relatively small disturbance to the system. Next, more severe disturbances are tested by decreasing the fault impedance Z_f. It is found that when Z_f is small, traditional methods will fail to converge, or converge to some non-practical solutions (as shown in Fig. 10). We have conducted more tests by selecting various Z_f values where $|Z_f| \in [0.01, 0.02]$, and compare the results obtained by TRAP, ME-NR, RK4-NR methods, respectively. Also, the three methods with initial values provided for Newton-Raphson by HE (actually the initial values are accurate enough for NR so that further NR iterations are not needed) are also tested. The results are shown in Fig. 11. It can be seen that without proper initial values, the conventional methods return highly inconsistent results, which reveal that NR method is not reliable. In contrast, by giving proper initial values, all the methods return consistent high-voltage solutions, and they are also consistent with the HE solution. To further verify the correctness of the HE results, the continuation approach is also used to solve the post-fault state, which gradually changes from the on-fault admittance matrix $\mathbf{Y}^-$ to the post-fault admittance matrix $\mathbf{Y}^+$ by adding a tiny increment $\Delta\mathbf{Y}_\varepsilon$ each time and solving the updated equations repeatedly [27]. The continuation approach uses 50 steps and reaches the same high-voltage solution as the HE derives. Thus, the consistency with the continuation approach result further verifies the correctness of the HE result.

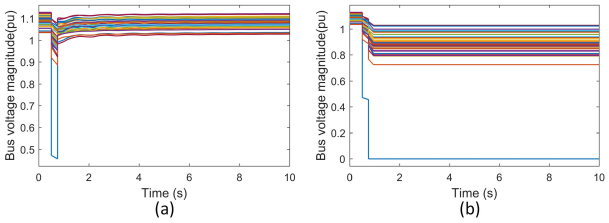

Fig. 10. Comparison of robustness. The fault is applied on bus 1 with $Z_f = j0.015$. (a) HE obtains correct system trajectory, while (b) ME-NR (Δt = 0.01 s) converges to a non-practical low-voltage solution.

When solving DAE, both differential and algebraic equations can induce computation errors. As shown in the test case above, HE can reduce the error from algebraic equations and avoid the non-convergence problems. Also, HE effectively reduces the cut-off errors from differential equations by providing higher-order approximate solutions, and thus achieves much larger time steps and higher efficiency.

C. 2383-bus Polish system

The proposed dynamic simulation method based on HE is demonstrated on the Polish test system with 2383 buses, 327

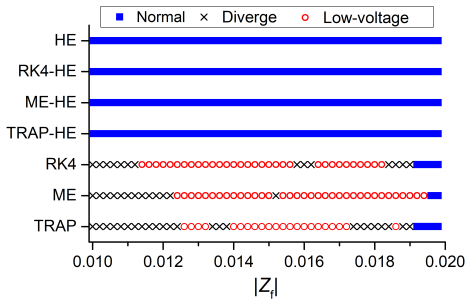

Fig. 11. Convergence profile of different methods on 39-bus system. TRAP-HE, ME-HE, RK4-HE use initial values provided by HE for Newton-Raphson methods. "Normal" means normal high-voltage solution, "Diverge" means NR fails to converge, "Low-voltage" means impractical, low-voltage solution.

synchronous generators with turbine governors and exciters, 1827 ZIP loads, and 1542 induction motors. The generators use 6th-order model. In the first case, we disarm all the controllers on the generators, apply 3-phase fault on bus 1396 at 0.5 s, and clear the fault at 0.95 s. The fault impedance $Z_f = j0.01$. In this case, the generator at bus 1140 accelerates significantly and finally runs out of step with the system. Fig. 12 shows the system dynamics simulated by HE. For the entire 5-s simulation, by setting $N_L = 15$, the HE takes 135.11 s to finish computation. Another case is multiple contingencies. The AVRs and TGs on the generators are activated, and the generators still use the 6th-order model. Double 3-phase faults are applied simultaneously on buses 42 and 540 at 0.5 s, and the faults are cleared at 0.75 s. Then another 3-phase fault is applied on bus 1396 at 1.5 s, and the fault is cleared at 1.95 s. All the faults are assumed to have impedance of $Z_f = j0.01$. With $N_L = 15$, the simulation of 10 s dynamics takes 92.69 s to finish. In comparison, the unstable case takes more computation time, this is because when system loses stability, the system states often change drastically (e.g. the rapid angle change shown in Fig. 12(d)), which causes reduced effective range of HE approximation.

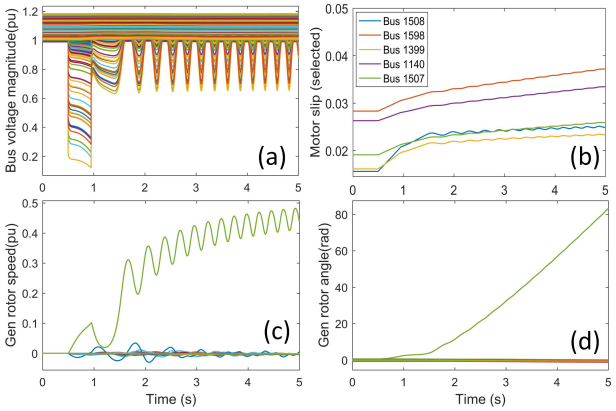

Fig. 12. Dynamics of Polish system simulated by HE (unstable). (a) voltage magnitude; (b) motor slip; (c) generator rotor speed; (d) generator rotor angle.

Note that all the conventional methods fail to converge when solving the post-fault states with NR method, so here HE is utilized for solving the post-switch states instead of NR method (HE only costs trivial portion computation time). To compare the accuracy of different methods, results from RK4 with tiny time step ($\Delta t = 2 \times 10^{-4}$ s) is set as the benchmark. Figs. 13 and 14 demonstrate errors of traditional methods (ME, RK4 and TRAP) with time step $\Delta t = 0.01$ s and HE in the unstable and stable cases, respectively. Table V compares the computation time of the methods. These results verify that HE has advantages both in accuracy and efficiency.

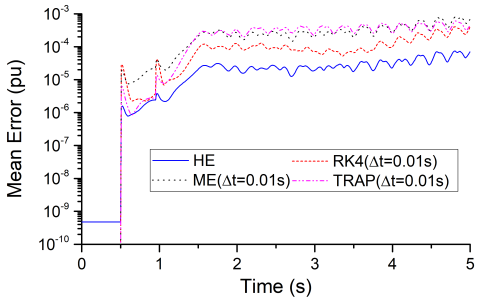

Fig. 13. Comparison of errors in Polish system (unstable case).

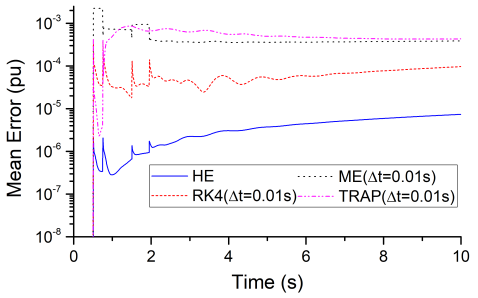

Fig. 14. Comparison of errors in Polish system (stable case).

TABLE V
COMPUTATION TIME OF DIFFERENT METHODS IN POLISH SYSTEM

Method	Time (s)	
	Unstable case (5s)	Stable case (10s)
ME (Δt = 0.01 s)	158.83	241.94
RK4 (Δt = 0.01 s)	288.34	510.82
TRAP (Δt = 0.01 s)	162.97	273.08
HE ($N_L = 15$)	135.11	92.69

The above tests in the Polish system verify the robustness and efficiency of HE in computing dynamics of large-scale systems. The HE can well handle stable and unstable cases and avoid numerical instability or divergence, which has significant advantages over traditional approaches in the analysis of complex nonlinear systems. In addition, the proposed approach can be utilized for more complex tasks, such as cascading outages [28] and controller placement [29].

This paper is mainly focused on the simulation of electro-mechanical transients. As a generic methodology, HE can also be applied to electromagnetic simulation. However, it has been observed that the timescales of the dynamics will also affect the time step of HE: the faster the dynamics are, the shorter

time step it requires. So for a stiff power system (e.g. with detailed modeling of power electronics), the issue may be similar with that encountered by conventional methods: the time step obtained by HE is limited and the computation is slowed down. However, as a higher-order approximation method, the effective time step of HE should still be larger than that of a conventional method. Moreover, necessary model simplifications should also be made to improve the efficiency e.g., use simplified equivalent models on components far from the fault location. Generally, the enhancement of performance may need both advanced simulation methodology and appropriate modeling practice. And the performance enhancement of HE regarding stiff systems will be our next research focus.

VII. Conclusion

This paper proposes a novel approach for dynamic simulation of power systems which enhances both efficiency and robustness of computation. The holomorphic embedding (HE) method is utilized to approximate the differential-algebraic equations (DAE) of the system, and generic rules for deriving the HE formulation are proposed. Within the generic HE computation framework, the HE modeling of synchronous generators and the treatment of transformation between generator and network coordinates are proposed. In addition, the HE formulations for solving the system states at the post-fault instant is proposed. Finally on the top level, the multi-stage HE is utilized to connect HE solutions into complete traces of system dynamics and to control the computation errors. With much larger effective time steps than traditional numerical integration methods, and non-iterative semi-analytical computation scheme of algebraic equations that avoids non-convergence issues, the HE has advantages over traditional simulation algorithms, both in efficiency and in robustness.

The proposed approach is tested on a 2-bus system, IEEE 39-bus system and the Polish 2383-bus system, respectively. By comparing with the commonly used modified Euler and Runge-Kutta with Newton-Raphson methods, and trapezoidal method, HE achieves less computation time as well as lower error. In addition, the HE avoids the common problem in Newton-Raphson method that the computation of algebraic equations does not converge when system is under stress or undergoes large disturbances. With enhanced efficiency and robustness, the proposed novel simulation approach is suitable for operational dynamic security assessment in practical systems. In addition, the proposed approach can be further utilized in cascading outage analysis, extended-term simulation of renewable energy integration and system restoration, which constitute our future work.

References

[1] H.-D. Chiang, *Direct methods for stability analysis of electric power systems: theoretical foundation, BCU methodologies, and applications*. John Wiley & Sons, 2011.

[2] M. Anghel, F. Milano, and A. Papachristodoulou, "Algorithmic construction of lyapunov functions for power system stability analysis," *IEEE Trans. Circuits Syst. I, Reg. Papers*, vol. 60, no. 9, pp. 2533–2546, 2013.

[3] P.-A. Lof, T. Smed, G. Andersson, and D. Hill, "Fast calculation of a voltage stability index," *IEEE Trans. Power Syst.*, vol. 7, no. 1, pp. 54–64, 1992.

[4] P. Maffezzoni, L. Codecasa, and D. D'Amore, "Time-domain simulation of nonlinear circuits through implicit runge–kutta methods," *IEEE Trans. Circuits Syst. I, Reg. Papers*, vol. 54, no. 2, pp. 391–400, 2007.

[5] Y. Liu, K. Sun, R. Yao, and B. Wang, "Power system simulation using a differential transformation method," *IEEE Trans. Power Syst.*, in press.

[6] H. Pulgar-Painemal, Y. Wang, and H. Silva-Saravia, "On inertia distribution, inter-area oscillations and location of electronically-interfaced resources," *IEEE Trans. Power Syst.*, vol. 33, no. 1, pp. 995–1003, 2018.

[7] B. Wang, N. Duan, and K. Sun, "A time-power series based semi-analytical approach for power system simulation," *IEEE Trans. Power Syst.*, vol. 34, no. 2, pp. 841–851, 2019.

[8] S. K. Khaitan, J. D. McCalley, and Q. Chen, "Multifrontal solver for online power system time-domain simulation," *IEEE Trans. Power Syst.*, vol. 23, no. 4, pp. 1727–1737, 2008.

[9] S. Jin *et al.*, "Comparative implementation of high performance computing for power system dynamic simulations," *IEEE Trans. Smart Grid*, vol. 8, no. 3, pp. 1387–1395, 2017.

[10] S.-K. Joo, C.-C. Liu, L. E. Jones, and J.-W. Choe, "Coherency and aggregation techniques incorporating rotor and voltage dynamics," *IEEE Trans. Power Syst.*, vol. 19, no. 2, pp. 1068–1075, 2004.

[11] J.-Y. Kim, J.-H. Jeon, S.-K. Kim, C. Cho, J. H. Park, H.-M. Kim, and K.-Y. Nam, "Cooperative control strategy of energy storage system and microsources for stabilizing the microgrid during islanded operation," *IEEE Trans. Power Electron.*, vol. 25, no. 12, pp. 3037–3048, 2010.

[12] R. Diao, V. Vittal, and N. Logic, "Design of a real-time security assessment tool for situational awareness enhancement in modern power systems," *IEEE Trans. Power Syst.*, vol. 25, no. 2, pp. 957–965, 2010.

[13] C.-W. Liu *et al.*, "New methods for computing power system dynamic response for real-time transient stability prediction," *IEEE Trans. Circuits Syst. I, Fundam. Theory Appl.*, vol. 47, no. 3, pp. 324–337, 2000.

[14] A. Trias, "The holomorphic embedding load flow method," in *Power and Energy Society General Meeting*. IEEE, 2012, pp. 1–8.

[15] H.-D. Chiang, T. Wang, and H. Sheng, "A novel fast and flexible holomorphic embedding method for power flow problems," *IEEE Trans. Power Syst.*, vol. 33, no. 3, pp. 2551–2562, 2018.

[16] C. Liu *et al.*, "Online voltage stability assessment for load areas based on the holomorphic embedding method," *IEEE Trans. Power Syst.*, vol. 33, no. 4, pp. 3720–3734, 2018.

[17] S. Rao and D. Tylavsky, "Nonlinear network reduction for distribution networks using the holomorphic embedding method," in *2016 North American Power Symposium (NAPS)*. IEEE, 2016, pp. 1–6.

[18] M. Basiri-Kejani and E. Gholipour, "Holomorphic embedding load-flow modeling of thyristor-based facts controllers," *IEEE Trans. Power Syst.*, vol. 32, no. 6, pp. 4871–4879, 2017.

[19] C. Liu, K. Sun, B. Wang, and W. Ju, "Probabilistic power flow analysis using multidimensional holomorphic embedding and generalized cumulants," *IEEE Trans. Power Syst.*, vol. 33, no. 6, pp. 7132–7142, 2018.

[20] C. Liu, N. Qin, K. Sun, and C. Leth Bak, "Remote voltage control using the holomorphic embedding load flow method," *IEEE Trans. Power Syst.*, in press.

[21] R. Yao and K. Sun, "Voltage stability analysis of power systems with induction motors based on holomorphic embedding," *IEEE Trans. Power Syst.*, vol. 34, no. 2, pp. 1278–1288, 2019.

[22] R. Yao, K. Sun, and F. Qiu, "Vectorized efficient computation of padé approximation for semi-analytical simulation of large-scale power systems," *IEEE Trans. Power Syst.*, in press.

[23] H. Stahl, "The convergence of padé approximants to functions with branch points," *Journal of Approximation Theory*, vol. 91, no. 2, pp. 139–204, 1997.

[24] S. Rao, Y. Feng, D. J. Tylavsky, and M. K. Subramanian, "The holomorphic embedding method applied to the power-flow problem," *IEEE Trans. Power Syst.*, vol. 31, no. 5, pp. 3816–3828, 2016.

[25] F. Milano, *Power system modelling and scripting*. Springer Science & Business Media, 2010.

[26] W. H. Press and S. A. Teukolsky, "Adaptive stepsize runge-kutta integration," *Computers in Physics*, vol. 6, no. 2, pp. 188–191, 1992.

[27] R. Yao, F. Liu, G. He, B. Fang, and L. Huang, "Static security region calculation with improved cpf considering generation regulation," in *IEEE International Conference on Power System Technology (POWERCON)*. IEEE, 2012, pp. 1–6.

[28] R. Yao, S. Huang, K. Sun, F. Liu, X. Zhang, and S. Mei, "A multi-timescale quasi-dynamic model for simulation of cascading outages," *IEEE Trans. Power Syst.*, vol. 31, no. 4, pp. 3189–3201, 2016.

[29] Y. Wang, H. D. Silva-Saravia, and H. A. Pulgar-Painemal, "Actuator placement for enhanced grid dynamic performance: A machine learning approach," *IEEE Trans. Power Syst.*, 2019.

Rui Yao (S'12–M'17) received the B.S. degree (with distinction) in 2011 and Ph.D. degree in 2016 in electrical engineering at Tsinghua University, Beijing, China. He was a postdoctoral research associate at the University of Tennessee, Knoxville during 2016–2018. He is currently a postdoctoral appointee at Argonne National Laboratory. His research interests include power system modeling and stability analysis, resilience modeling and assessment, and high-performance computational methodologies.

Yang Liu (S'17) received the B.S. degree in energy and power engineering from Xian Jiaotong University, China, in 2013, and the M.S. degree in power engineering from Tsinghua University, China, in 2016, respectively. He is currently pursuing the Ph.D. degree at the Department of Electrical Engineering and Computer Science, University of Tennessee, Knoxville, USA. His research interests include power system simulation, stability and control.

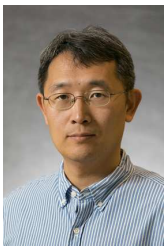

Kai Sun (M'06–SM'13) received the B.S. degree in automation in 1999 and the Ph.D. degree in control science and engineering in 2004 both from Tsinghua University, Beijing, China. He is an associate professor at the Department of EECS, University of Tennessee, Knoxville, USA. He was a project manager in grid operations and planning at the EPRI, Palo Alto, CA from 2007 to 2012. Dr. Sun serves in the editorial boards of IEEE Transactions on Power Systems, IEEE Transactions on Smart Grid, IEEE Access and IET Generation, Transmission and Distribution.

Feng Qiu (M'14–SM'18) received the Ph.D. degree from the School of Industrial and Systems Engineering, the Georgia Institute of Technology, Atlanta, Georgia, in 2013. He is a computational scientist with the Energy Systems Division at Argonne National Laboratory, Lemont, IL, USA. His current research interests include optimization in power system operations, electricity markets, and power grid resilience.

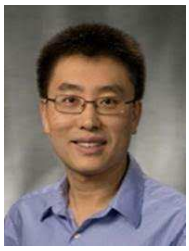

Jianhui Wang (M'07–SM'12) received the Ph.D. degree in electrical engineering from Illinois Institute of Technology, Chicago, Illinois, USA, in 2007.

Presently, he is an Associate Professor with the Department of Electrical and Computer Engineering at Southern Methodist University, Dallas, Texas, USA. Prior to joining SMU, Dr. Wang had an eleven-year stint at Argonne National Laboratory with the last appointment as Section Lead – Advanced Grid Modeling. Dr. Wang is the secretary of the IEEE Power & Energy Society (PES) Power System Operations, Planning & Economics Committee. He has held visiting positions in Europe, Australia and Hong Kong including a VELUX Visiting Professorship at the Technical University of Denmark (DTU). Dr. Wang is the Editor-in-Chief of the IEEE Transactions on Smart Grid and an IEEE PES Distinguished Lecturer. He is also a Clarivate Analytics highly cited researcher for 2018.